AIMS Bioengineering, 9(2): 213–238.
DOI: 10.3934/bioeng.2022015
Received: 22 December 2021
Revised: 09 May 2022
Accepted: 22 June 2022
Published: 27 June 2022

http://www.aimspress.com/journal/Bioengineering

Research article

Coupled effects of channels and synaptic dynamics in stochastic modelling of healthy and Parkinson's-disease-affected brains

Thi Kim Thoa Thieu[1,*] **and Roderick Melnik**[1,2]

[1] M3AI Laboratory, MS2Discovery Interdisciplinary Research Institute, Wilfrid Laurier University, Waterloo, Ontario, Canada

[2] BCAM - Basque Center for Applied Mathematics, Bilbao, Spain

* **Correspondence:** Email: tthieu@wlu.ca.

Abstract: Our brain is a complex information processing network in which the nervous system receives information from the environment to quickly react to incoming events or learns from experience to sharp our memory. In the nervous system, the brain states translate collective activities of neurons interconnected via synaptic connections. In this paper, we study coupled effects of channels and synaptic dynamics under the stochastic influence of healthy brain cells with applications to Parkinson's disease (PD). In particular, we investigate the effects of random inputs in a subthalamic nucleus (STN) cell membrane potential model. The STN bursting phenomena and parkinsonian hypokinetic motor symptoms are closely connected, as electrical and chemical maneuvers modulating STN bursts are sufficient to ameliorate or mimic parkinsonian motor deficits. Deep brain stimulation (DBS) of the STN is an important surgical technique used in the treatment to improve PD symptoms. Our numerical results show that the random inputs strongly affect the spiking activities of the STN neuron not only in the case of healthy cells but also in the case of PD cells in the presence of DBS treatment. Specifically, the existence of a random refractory period together with random input current in the system may substantially influence an increased irregularity of spike trains of the output neurons.

Keywords: neurodegenerative disorders; coupled synaptic connections; damaged cells; burst discharges; systems with random fluctuations; deep brain stimulation; parkinsonian symptoms; neuronal feedback; stochastic models

1. Introduction

One of the most common age-associated human neurodegenerative disorders is Parkinson's disease (PD). PD is characterized by cardinal motor symptoms such as static tremor, bradykinesia, and muscle rigidity. Many different treatments focus on the subthalamic nucleus (STN) to improve

such motor symptoms, for instance, ablation surgery of STN or its fiber connections. Deep brain stimulation (DBS) of the STN has recently become an effective therapy of PD [1]. The DBS is a very impressive method [2] due to the fact that PD, characterized by the inadequacy of a chemical substance in the brain, can also be successfully treated with passage of only electrical currents without concomitant supply of biological or chemical reactions/factors. In general, biological neurons in the brains transmit information by generating spikes and such neurons are connected by synapses that process and store information. To better understand the brain activities, therefore, we need to know how synapses work [3]. Many models have been proposed to analyze the dynamics of synaptic coupling of human brains in neurodegenerative disorders and therapeutic targets for such diseases (e.g., [4] and references therein). In particular, a model of T-type Ca2+ channels as a new therapeutic target for Parkinson's disease has been proposed in [1]. The authors in [5] have shown that subthalamic burst discharges play an imperative role in cortico-subcortical information relay, and they critically contribute to the pathogenesis of both hypokinetic and hyperkinetic parkinsonian symptoms. The role of the CaV1.3 channels in calcium and iron uptake in the context of pharmacological targeting for improving the PD pathology has been discussed in [6]. A review [7] gives the evaluation of the therapeutic potential of L-type calcium channels (LTCC), R-type calcium channels (RTCC), and T-type calcium channels (TTCC) inhibition in light of novel preclinical and clinical data and the feasibility of available Ca2+ channel blockers to modify PD progression. The authors in [8] have considered an engineering selectivity into RGK (Rad, Rem, Rem2, Gem/Kir) GTPase inhibition of voltage-dependent calcium channels that is in connection with treatment strategies for diseases including chronic pain and Parkinson's disease. Beside the effects of calcium channels on PD, the potassium (K+) channels also play an important role in managing and controlling the PD. There are several results available along this line. In particular, the authors in [5] have shown that subthalamic burst discharges are dependent on input from the motor cortex, causing erroneous re-entrant information relays from corticosubthalamic to pallido-thalamocortical loops and thus parkinsonian tremors. In [9], the authors have summarized the physiological and pharmacological effects of three K+ channels as a potential therapeutic target for PD. The effects of pharmacological blockade or activation of K+ channels in the progression and treatment of PD have been discussed in [10].

To get closer to the real scenarios in the application of neuronal models for PD, we should account for the existence of random fluctuations in the system. Specifically, the stochastic inputs arise through sensory fluctuations, brainstem discharges and thermal energy as well as random fluctuations at a microscopic level, such as the Brownian motion of ions. The stochasticity can arise even from the devices which are used for medical treatments, e.g. devices for injection currents in DBS. The authors in [11] have shown that brain rhythm bursts are enhanced by multiplicative noise. The presence of noise in gamma oscillations in a model of neuronal networks with different reversal potentials has been reported in [12]. However, the presence of random factors is not always disadvantageous, such noisy factors can also bring benefits to nervous systems. The noises in the neuronal system are not only a problem for neurons, they can also be a solution in information processing [13, 14]. The detectability of weak signals in nonlinear systems (a phenomenon known as stochastic resonance) can be enhanced by random noise [15]. The authors in [15] have also indicated that the phase-based simplification of the STN neurons can accurately predict responses to temporally complex trains of inputs even when the perturbations in timing are large enough to obscure the oscillatory nature of the neuron's firing.

Taking the inspiration from the fields of PD studies together with the effects of natural random

factors in biological system dynamics, we develop and investigate a model of coupled effects of channels and synaptic dynamics by using stochastic modelling of healthy brain cells with applications in PD. In particular, we consider a cell membrane potential model in the STN part of the human brain. Our analysis focuses on considering a Langevin stochastic equation in a numerical setting for a cell membrane potential with random inputs. We provide numerical examples and discuss the effects of random inputs on the time evolution of the STN cell membrane potential as well as the spiking activities of the STN neuron. Furthermore, we know that the STN bursting phenomenon is one of the main factors that cause parkinsonian hypokinetic motor symptoms, whereas. DBS is a surgical technique used in the treatment to improve PD. Our numerical results show that random inputs strongly affect the spiking activities in the STN neuron in the absence and in the presence of DBS.

2. Model description

The second most common neurodegenerative disease after Alzheimer's disease is PD. PD is caused by naturally occurring proteins that fold into the wrong shape and stick together with other proteins, eventually forming thin filament-like structures called amyloid fibrils. Researchers in [16] have found that calcium influences the way alpha-synuclein proteins interact with synaptic vesicles. In fact, alpha-synuclein is almost like a calcium sensor. In the presence of calcium, alpha-synyclein changes its structure and the way interacts with its environment, which is likely to be very important for its normal function. In nervous systems, calcium channels play an important role in the release of neurotransmitters. In particular, when the level of calcium in the nerve cell increases, the alpha-synuclein binds to synaptic vesicles at multiple points causing the vesicles to come together. The normal role of alpha-synuclein is to help the chemical transmission of information across nerve cells. Losing dopaminergic (DA) midbrain neurons within the substantia nigra (SN) can cause prevalent movement disorder. One of the most prevalent disorders is PD. In general, a significant increase of the calcium currents in the neuronal system could cause burst discharges in STN. This phenomenon of burst discharges is linked to the loss of DA neurons in the midbrain STN. Therefore, in our model, taking the inspiration from [17], we consider a low-threshold calcium current together with a calcium-activated potassium channel to reduce the effects of calcium currents in the system.

Furthermore, motivated by [1, 9, 10, 17], we consider a modified Hodgkin-Huxley (HH) system modelling a STN cell membrane potential. In particular, we choose first a STN healthy cell, then switch to a PD cell, and study the effects of random inputs on the STN cell membrane potential under synaptic conductance dynamics.

In biological systems of brain networks, instead of physically joined neurons, a spike in the presynaptic cell causes a release of a chemical, or a neurotransmitter. Neurotransmitters are released from synaptic vesicles into a small space between the neurons called the synaptic cleft [18]. In what follows, we will focus on investigating the chemical synaptic transmission and study how excitation and inhibition affect the patterns in the neurons' spiking output in our HH model.

In this section, we consider a HH model of synaptic conductance dynamics. In particular, neurons receive a myriad of excitatory and inhibitory synaptic inputs at dendrites. To better understand the mechanisms of synaptic conductance dynamics, we use the description of Poissonian trains to investigate the dynamics of the random excitatory (E) and inhibitory (I) inputs to a neuron [19, 20].

We consider the transmitter-activated ion channels as an explicitly time-dependent conductivity ($g_{\text{syn}}(t)$). The conductance transients can be defined by the following equation (see, e.g., [18, 19]):

$$\frac{dg_{\text{syn}}(t)}{dt} = -\bar{g}_{\text{syn}} \sum_k \delta(t - t_k) - \frac{g_{\text{syn}}(t)}{\tau_{\text{syn}}}, \tag{2.1}$$

where $\bar{g}_{\text{syn}}$ (synaptic weight) denotes the maximum conductance elicited by each incoming spike, while τ_{syn} is the synaptic time constant, and $\delta(\cdot)$ is the Dirac delta function. Note that the summation runs over all spikes received by the neuron at time t_k. We have the following formula for converting conductance changes to the current by using Ohm's law:

$$I_{\text{syn}}(t) = g_{\text{syn}}(t)(V(t) - E_{\text{syn}}), \tag{2.2}$$

where V is the membrane potential, while E_{syn} represents the direction of current flow and the excitatory or inhibitory nature of the synapse.

The total synaptic input current I_{syn} is the combination of both excitatory and inhibitory inputs. Assume that the total excitatory and inhibitory conductances received at time t are $g_E(t)$ and $g_I(t)$, and their corresponding reversal potentials are E_E and E_I, respectively. Then, the total synaptic current can be defined by the following equation (see, e.g., [20]):

$$I_{\text{syn}}(V(t), t) = -g_E(t)(V - E_E) - g_I(t)(V - E_I) = -I_{\text{E}} - I_{\text{I}}. \tag{2.3}$$

In [17], the authors have used the quantity $I_{\text{GPe,STN}}$ in the STN model. However, we know that STN-DBS generate both excitatory and inhibitory postsynaptic potentials in STN neurons [21]. In our current consideration, instead of using the current $I_{\text{GPe,STN}}$, we consider the current $I_{\text{STN,DBS}} = -I_{\text{E}} - I_{\text{I}}$. Let us define the following synaptic dynamics of the STN cell membrane potential (V) described by the following model (based on [17])

$$C_m \frac{d}{dt} V(t) = -I_L - I_{\text{Na}} - I_{\text{K}} - I_{\text{T}} - I_{\text{Ca}} - I_{\text{ahp}} - I_{\text{STN,DBS}} + I_{\text{app}} + I_{\text{dbs}} \quad \text{if } V(t) \le V_{\text{th}}, \tag{2.4}$$

$$V(t) = V_{\text{reset}} \quad \text{otherwise}, \tag{2.5}$$

where I_{app} is the external input current, while C_m is the membrane capacitance and $t \in [0, T]$. Additionally, in (2.4), V_{th} denotes the membrane potential threshold to fire an action potential.

In this model, we assume that a spike takes place whenever $V(t)$ crosses V_{th} in the STN membrane potential. In that case, a spike is recorded and $V(t)$ resets to V_{reset} value. Hence, the reset condition is summarized by $V(t) = V_{\text{reset}}$ if $V(t) \geq V_{\text{th}}$. The quantity I_{ahp} represents the calcium-activated potassium current for the spike after hyperpolarization in STN.

The concentration of intracellular Ca2+ is governed by the following calcium balance equation

$$\frac{d}{dt}Ca(t) = \varepsilon(I_{\text{Ca}} - I_T - k_{\text{Ca}}\text{Ca}(t)), \tag{2.6}$$

where $\varepsilon = 3.75 \times 10^{-5}$ is a scaling constant, $k_{\text{Ca}} = 22.5$ (ms^{-1}) is a given time constant (see, e.g., [22, 23]).

Furthermore, we consider an external random (additive noise) input current as follows: $I_{\text{app}} = \mu_{\text{app}} + \sigma_{\text{app}}\eta(t)$, where η is the zero-Gaussian white noise with $\mu_{\text{app}} > 0$ and $\sigma_{\text{app}} > 0$. Using the description of such random input current in our system, the first equation (2.4) can be considered as the following Langevin stochastic equation (see, e.g., [24]):

$$C_m\frac{d}{dt}V(t) = -I_L - I_{\text{Na}} - I_{\text{K}} - I_{\text{T}} - I_{\text{Ca}} - I_{\text{ahp}} - I_{\text{E}} - I_{\text{I}} + I_{\text{dbs}} + \mu_{\text{app}} + \sigma_{\text{app}}\eta(t) \quad \text{if } V(t) \leq V_{\text{th}}. \tag{2.7}$$

Therefore, the system (2.4)–(2.6) ($t \in [0, T]$) can be rewritten as

$$C_m\frac{d}{dt}V(t) = -I_L - I_{\text{Na}} - I_{\text{K}} - I_{\text{T}} - I_{\text{Ca}} - I_{\text{ahp}} - I_{\text{E}} - I_{\text{I}} + I_{\text{dbs}} + \mu_{\text{app}} + \sigma_{\text{app}}\eta(t) \quad \text{if } V(t) \leq V_{\text{th}}, \tag{2.8}$$

$$V(t) = V_{\text{reset}} \quad \text{otherwise.} \tag{2.9}$$

Furthermore, we consider the following gating variable dynamics (see, e.g., [17])

$$\frac{d}{dt}h(t) = 0.75\frac{h_\infty(V) - h(t)}{\tau_h(V)}, \tag{2.10}$$

$$\frac{d}{dt}n(t) = 0.75\frac{n_\infty(V) - n(t)}{\tau_n(V)}, \tag{2.11}$$

$$\frac{d}{dt}r(t) = 0.2\frac{r_\infty(V) - r(t)}{\tau_r(V)}, \tag{2.12}$$

$$\frac{d}{dt}c(t) = 0.08\frac{c_\infty(V) - c(t)}{\tau_c(V)}, \tag{2.13}$$

$$\frac{d}{dt}Ca(t) = \varepsilon(I_{\text{Ca}} - I_T - k_{\text{Ca}}\text{Ca}(t)). \tag{2.14}$$

The initial data we use for the system (2.8)–(2.14) define its initial conditions:

$$V(0) = V_0, \tag{2.15}$$
$$h(0) = h_\infty(V_0), \tag{2.16}$$
$$n(0) = n_\infty(V_0), \tag{2.17}$$
$$r(0) = r_\infty(V_0), \tag{2.18}$$
$$c(0) = c_\infty(V_0), \tag{2.19}$$
$$Ca(0) = \frac{a_\infty(V_0)}{a_\infty(V_0) + b_\infty(V_0)}, \tag{2.20}$$

where $h_\infty, n_\infty, r_\infty, c_\infty, a_\infty, b_\infty$ are described as in Table 1.

In our model (2.8)–(2.20), as we mentioned above, we use the simplest input spike train with Poisson process in which the stochastic process of interest provides a suitable approximation to stochastic neuronal firings [25]. The input spikes will be carried out by the quantity $\sum_k \delta(t - t_k)$ in the equation (2.1) and the input spikes are given when every input spike arrives independently of other spikes. The process will be described as follows:

- For designing a spike generator of spike train, we define the probability of firing a spike within a short interval (see, e.g. [19]) as $P(1 \text{ spike during } \Delta t) = r_j \Delta t$, where $j = e, i$ with r_e, r_i representing the instantaneous excitatory and inhibitory firing rates, respectively.
- Then, a Poisson spike train is generated by first subdividing the time interval into a group of short sub-intervals through small time steps Δt. In our model, we use $\Delta t = 0.1$ (ms).
- We define a random variable x_{rand} with uniform distribution over the range between 0 and 1 at each time step.
- Finally, we compare the random variable x_{rand} with the probability of firing a spike, which reads:

$$\begin{cases} r_j \Delta t > x_{\text{rand}}, \text{ generates a spike,} \\ r_j \Delta t \le x_{\text{rand}}, \text{ no spike is generated.} \end{cases} \tag{2.21}$$

By using model (2.8)–(2.20), we also investigate the effects of random refractory periods. We consider the random refractory periods t_{ref} as $t_{\text{ref}} = \mu_{\text{ref}} + \sigma_{\text{ref}} \tilde{\eta}(t)$, where $\tilde{\eta}(t) \sim \mathcal{N}(0, 1)$ is the standard normal distribution, $\mu_{\text{ref}} > 0$ and $\sigma_{\text{ref}} > 0$.

In general, the information on stimulating activities in a neuron can be provided by the irregularity of spike trains. The time interval between adjacent spikes is called the inter-spike-interval (ISI). The coefficient of variation (CV) of the ISI in a cell membrane potenial with multiple inputs can bring useful information about the output of a decoded neuron. In what follows, we will demonstrate that when we increase the value of σ_{ref}, the irregularity of the spike trains increases (see also [26]).

The spike irregularity of spike trains can be described via the coefficient of variation of the inter-spike-interval (see, e.g., [26, 27]) as follows:

$$CV_{\text{ISI}} = \frac{\sigma_{\text{ISI}}}{\mu_{\text{ISI}}}, \tag{2.22}$$

where σ_{ISI} is the standard deviation and μ_{ISI} is the mean of the ISI of an individual neuron.

In the next section, let us consider the output firing rate as a function of Gaussian white noise mean or direct current value, namely, the input-output transfer function of the neuron.

In our model, we choose the parameter set as in the following Table 1:

Table 1. Steady-state functions for channel gating variables and time constants for the different ion channels (see, e.g., [17]).

Current	Gating variables	Gating variables	Parameters
$I_{\text{L}} = g_L(v - E_{\text{L}})$			$g_L = 2.25$ (nS)
			$E_{\text{L}} = -60$ (mV)
$I_{\text{Na}} = g_{\text{Na}} m_\infty^3(V) h(V)(V - E_{\text{Na}})$	$m_\infty(V) = 1/(1 + \exp(-\frac{V+30}{15}))$	$h_\infty(V) = 1/(1 + \exp(-\frac{V+39}{3.1})$	$g_{\text{Na}} = 37$
		$\tau_h(V) = 1 + 500/(1 + \exp(-\frac{V+57}{-3})$	$E_{\text{Na}} = 55$ (mV)
$I_{\text{K}} = g_{\text{K}} n^4(V)(V - E_{\text{K}})$	$n_\infty(V) = 1/(1 + \exp(-\frac{V+32}{8}))$		$g_{\text{K}} = 45$ (nS)
	$\tau_n(V) = 1 + 100/(1 + \exp(-\frac{V+80}{-26})$		$E_{\text{K}} = -80$ (mV)
$I_{\text{T}} = g_{\text{T}} a_\infty^3(V) b_\infty^2(r) r(V)(V - E_{\text{T}})$	$a_\infty(V) = 1/(1 + \exp(-\frac{V+63}{7.8}))$	$r_\infty(V) = 1/(1 + \exp(\frac{V+67}{2})$	$g_{\text{T}} = 0.5$ (nS)
	$b_\infty(V) = 1/(1 + \exp(-\frac{V-0.4}{0.1}))$	$\tau_r(V) = 7.1 + 17.5/(1 + \exp(-\frac{V+68}{-2.2})$	$E_{\text{T}} = 0$ (mV)
	$-1/(1 + \exp(4))$		
$I_{\text{Ca}} = g_{\text{Ca}} c^2(V)(V - E_{\text{Ca}})$	$c_\infty(V) = 1/(1 + \exp(-\frac{V+20}{8}))$		$g_{\text{Ca}} = 2$ (nS)
	$\tau_c(V) = 1 + 10/(1 + \exp(\frac{V+80}{26})$		$E_{\text{Ca}} = 140$ (mV)
$I_{\text{ahp}} = g_{\text{ahp}}(V - E_{\text{ahp}})(\frac{\text{Ca}}{\text{Ca}+15})$			$g_{\text{ahp}} = 20$ (nS)
			$E_{\text{ahp}} = -80$ (mV)
$I_{\text{dbs}} = 5 + 5\sin(2\pi t)$ (pA)			

Since these parameters have also been used in [17] for STN cell membrane potential experiments, we take them for our model validation. Moreover, in our consideration, we use not only the parameters from Table 1, but also the following parameters: $V_{\text{th}} = -55$ (mV), $V_{\text{reset}} = -70$ (mV), $V_0 = -65$ (mV), $\Delta t = 0.1$, $C_m = 10$ (nF), $\tau_E = 2$ (ms), $\tau_I = 5$ (ms), $\bar{g}_E = 1.5$ (nS), $\bar{g}_I = 0.5$ (nS), $r_e = 10$, $r_i = 10$, $n_E = 20$ spike trains, $n_I = 80$ spike trains. Here, n_E and n_I represent the number of excitatory and inhibitory presynaptic spike trains, respectively.

Mathematically, the developed model (2.8)–(2.20) is an evolutionary system that combines stochastic differential equations and ordinary differential equations (SDEs-ODEs), where the stochastic membrane potential equation is coupled to the activation and inactivation ion channels equations, as well as to the calcium-activated potassium current equation. This system can be considered as a modified HH system.

Models proposed in [17] represent the responses of STN neurons to the depolarization of current injection with repetitive firing and exhibit rebound bursts with more rapid de-activation of T-type calcium currents I_{T}. However, in their models, they consider a modified version of a basal Ganglia-Thalamic network model with a special focus on the dynamics of membrane potentials in a deterministic case. In real-world applications, the stochastic factors become important in capturing the effects of ion channels. Taking the inspiration from the studies in [24, 28], our focus in the remainder of this paper will be on the effects of random inputs on a STN cell membrane potential

under synaptic dynamics with applications in PD. In general, the external current controls the firing mode in neuronal systems. A wrong thalamic transmission could lead to errors such as misses, bursts and/or spurious events. Moreover, the contribution of random factors could reduce the response of the neuron to each stimulus in the STN. In the next section, we will be analyzing the effects of Gaussian white noise input current and random refractory periods on the spiking activities in a STN cell membrane potential in the absence and in the presence of DBS.

3. Numerical results

In this section, we take a single STN neuron and study how the neuron behaves under random inputs and when it is bombarded with both excitatory and inhibitory spike trains. The numerical results reported in this section are obtained by using a discrete-time integration based on the Euler method implemented in Python.

In particular, we use the coupled SDEs-ODEs system (2.8)–(2.20) that describes the dynamics of the STN membrane potential. As we have mentioned in the previous section, we will focus on the effects of Gaussian white noise input current together with the random refractory periods on the STN cell membrane potential.

In what follows, we use the excitatory and inhibitory conductances provided in Figure 1 for all of our simulations. The main numerical results of our analysis are shown in Figures 2–16, where we have plotted the time evolution of the membrane potential calculated based on model (2.8)–(2.20), along with the spike count profile and the corresponding spike irregularity profile. We investigate the effects of additive type of random input currents in presence of a random refractory period in a modified HH neuron under synaptic conductance dynamics. We observe that with a Poissonian spike input, the random external currents and random refractory period influence the spiking activity of a neuron in the cell membrane potential.

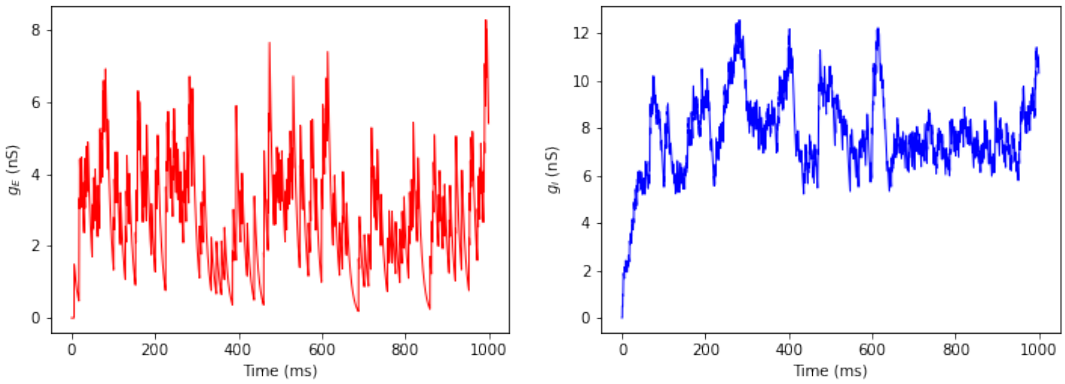

Figure 1. Left: Excitatory conductances profile corresponding to the dynamics (2.1). Right: Inhibitory conductances profile corresponding to the dynamics (2.1).

In order to switch from healthy conditions to Parkinsonian conditions in the basal ganglia model, we consider a decrease in the current I_{app} applied to the STN. In particular, we have $I_{\text{app}} = 33$ (pA) for a healthy STN cell and $I_{\text{app}} = 23$ (pA) for a Parkinsonian STN cell (see, e.g., [17]). Therefore, a STN cell in the case of injected current input $I_{\text{app}} = 33$ (pA) results in a healthy STN cell, while a STN cell

in the case of injected current $I_{\text{app}} = 23$ (pA) is considered as a PD-affected STN cell.

In Figure 2, we have plotted the Gaussian white noise current profile, the time evolution of the membrane potential $V(t)$ with various input values of currents and refractory period for the case of a healthy STN cell ($I_{\text{app}} = 33$ (pA)), see e.g. in [17]. In the second row of Figure 2, we plot the time evolution of the membrane potential under an additive type of random input current $I_{\text{app}} = 33 + \eta(t)$ (pA) together with a random refractory period $t_{\text{ref}} = 3 + \sigma_{\text{ref}}\tilde{\eta}(t)$ (ms). As expected, we obsevere that there are fluctuations in the time evolution of the membrane potential. Note that a miss state occurs when a neuron is failed to spike, whereas when the state of a neuron spikes more than once within 25 (ms) we observe a burst (see, e.g., [17]). In the last three rows of Figure 2, there exist missing moods in the behavior of the membrane potential (e.g., from time equal to 300 to 500 (ms)). This is caused by the presence of the additive noise input current and the random refractory period in the system. This is visible also in the last two rows of Figure 2, but the fluctuations are smaller than the case shown in the second row of the same figure. Further analysis of the last two rows of Figure 2 in the case of direct input currents reveals that the time evolution of the membrane potential looks similar in both cases: direct and random refractory periods.

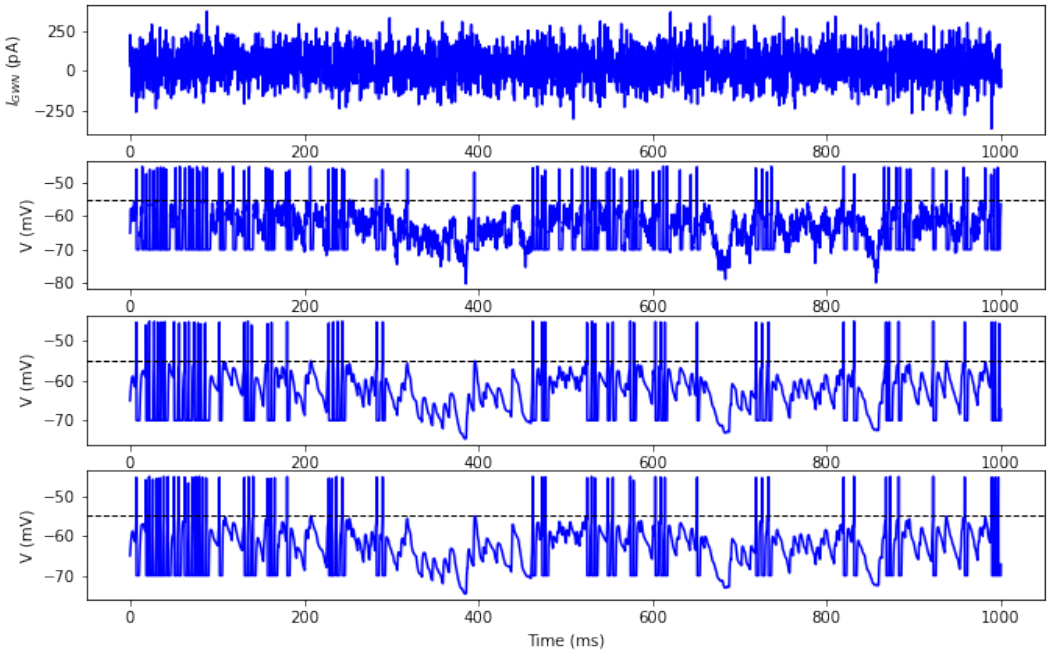

Figure 2. First row: Gaussian white noise current profile. Second row: Time evolution of membrane potential $V(t)$ with additive noise current $I_{\text{app}} = 33 + \eta(t)$ (pA) and random refractory period $t_{\text{ref}} = 3 + \sigma_{\text{ref}}\tilde{\eta}(t)$ (ms). Third row: Time evolution of membrane potential $V(t)$ with direct input current $I_{\text{app}} = 33$ (pA) and with random refractory period $t_{\text{ref}} = 3 + \sigma_{\text{ref}}\tilde{\eta}(t)$ (ms). Fourth row: Time evolution of membrane potential $V(t)$ with direct input current $I_{\text{app}} = 33$ (pA) and with direct refractory period $t_{\text{ref}} = 3$ (ms). Parameters: $\sigma_{\text{ref}} = 0.5$, $I_{\text{dbs}} = 0$ (pA). The dash line represents the spike threshold $V_{\text{th}} = -55$ (mV).

In Figure 3, we switch from the healthy condition to the Parkinsonian condition by decreasing the value of I_{app} compared to the previous cases in Figure 2. In particular, in the second row of Figure 3, we consider the time evolution of membrane potential $V(t)$ with additive noise current $I_{\text{app}} = 23 + \eta(t)$ (pA) and random refractory period $t_{\text{ref}} = 3 + \tilde{\eta}(t)$ (ms). We observe that there is an increase in the missing moods in the time evolution of the membrane potential in all last three rows. Moreover, there still exist fluctuations in the second row of Figure 3 because of the presence of additive noise input current and a random refractory period in the system.

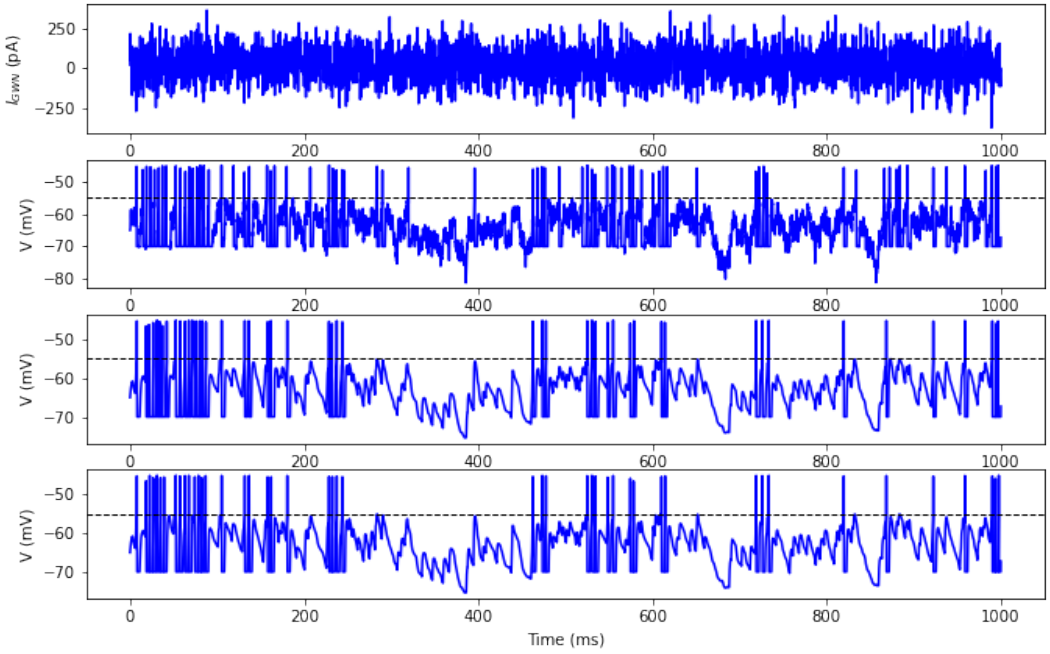

Figure 3. First row: Gaussian white noise current profile. Second row: Time evolution of membrane potential $V(t)$ with additive noise current $I_{\text{app}} = 23 + \eta(t)$ (pA) and random refractory period $t_{\text{ref}} = 3 + \tilde{\eta}(t)$ (ms). Third row: Time evolution of membrane potential $V(t)$ with direct input current $I_{\text{app}} = 23$ (pA) and with random refractory period $t_{\text{ref}} = 3 + \tilde{\eta}(t)$ (ms). Fourth row: Time evolution of membrane potential $V(t)$ with direct input current $I_{\text{app}} = 23$ (pA) and with direct refractory period $t_{\text{ref}} = 3$ (ms). Parameters: $\sigma_{\text{ref}} = 0.5$, $I_{\text{dbs}} = 0$ (pA). The dash line represents the spike threshold $V_{\text{th}} = -55$ (mV).

In order to reduce the misses in the cases presented in Figure 3, we applied intracellularly a DBS frequency input current $I_{\text{dbs}} = 5 + 5\sin(2\pi t)$ (pA) to the STN cell, as shown in Figure 4. It is clear that the spiking activities increase in the last three rows of Figure 4. The cases presented in Figure 4 look similar to the cases of the healthy STN cell presented in Figure 3. There are fluctuations in the last three rows of Figure 4 due to the presence of random factors.

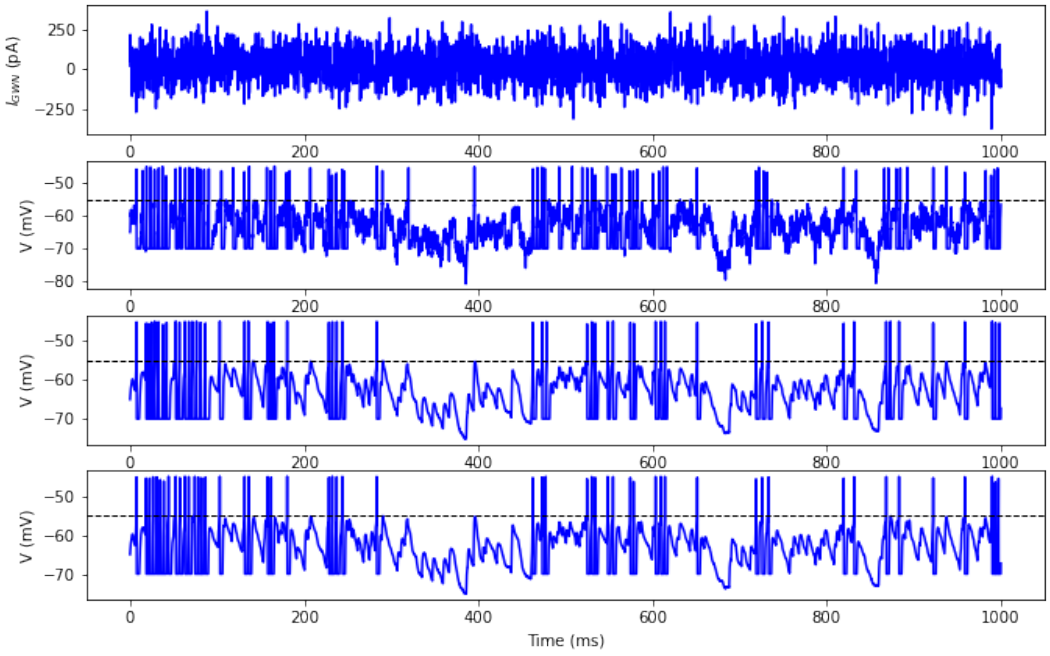

Figure 4. First row: Gaussian white noise current profile. Second row: Time evolution of membrane potential $V(t)$ with additive noise current $I_{\text{app}} = 23 + \eta(t)$ (pA) and random refractory period $t_{\text{ref}} = 3 + \tilde{\eta}(t)$ (ms). Third row: Time evolution of membrane potential $V(t)$ with direct input current $I_{\text{app}} = 23$ (pA) and with random refractory period $t_{\text{ref}} = 3 + \tilde{\eta}(t)$ (ms). Fourth row: Time evolution of membrane potential $V(t)$ with direct input current $I_{\text{app}} = 23$ (pA) and with direct refractory period $t_{\text{ref}} = 3$ (ms). Parameters: $\sigma_{\text{ref}} = 0.5$, $I_{\text{dbs}} = 5 + 5\sin(2\pi t)$ (pA). The dash line represents the spike threshold $V_{\text{th}} = -55$ (mV).

Next, we increase the value of σ_{ref} from 0.5 to 2 for the cases presented in Figures 5–7. Specifically, in the presence of a random refractory period with $\sigma_{\text{ref}} = 2$, the misses and bursts are slightly increased in the second and third rows of Figure 5, while the time evolutions in the last two rows look more stable. In the presence of a random refractory period together with a large enough value of σ_{ref}, the healthy conditions may be switched to the Parkinsonian conditions even without decreasing the value of I_{app}. This is due to the fact that the presence of random factors could contribute to the changes in neuron responses in a cell membrane potential.

In Figure 6, we consider similar quantities as in the cases presented in Figure 5. The only difference is that we decrease the values of I_{app}. We observe that the silence moods seem to be increased more than in the cases presented in the second and third rows of Figure 5.

Similarly, we add a DBS frequency input current to the system to reduce the misses in the STN cell. In particular, in Figure 7, we see that the presence of the DBS frequency input current leads to a significant increase in the spiking activity of the STN neuron. The cases presented in Figure 7 looks similar to the cases with healthy STN cells presented in Figure 5.

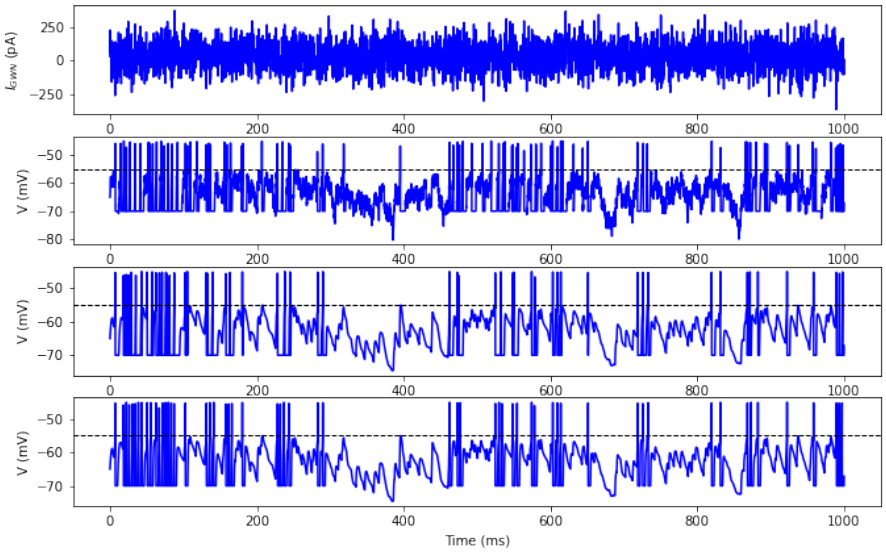

Figure 5. First row: Gaussian white noise current profile. Second row: Time evolution of membrane potential $V(t)$ with additive noise current $I_{\text{app}} = 33 + \eta(t)$ (pA) and random refractory period $t_{\text{ref}} = 3 + \sigma_{\text{ref}}\tilde{\eta}(t)$ (ms). Third row: Time evolution of membrane potential $V(t)$ with direct input current $I_{\text{app}} = 33$ (pA) and with random refractory period $t_{\text{ref}} = 3 + \sigma_{\text{ref}}\tilde{\eta}(t)$ (ms). Fourth row: Time evolution of membrane potential $V(t)$ with direct input current $I_{\text{app}} = 33$ (pA) and with direct refractory period $t_{\text{ref}} = 3$ (ms). Parameters: $\sigma_{\text{ref}} = 2$, $I_{\text{dbs}} = 0$ (pA). The dash line represents the spike threshold $V_{\text{th}} = -55$ (mV).

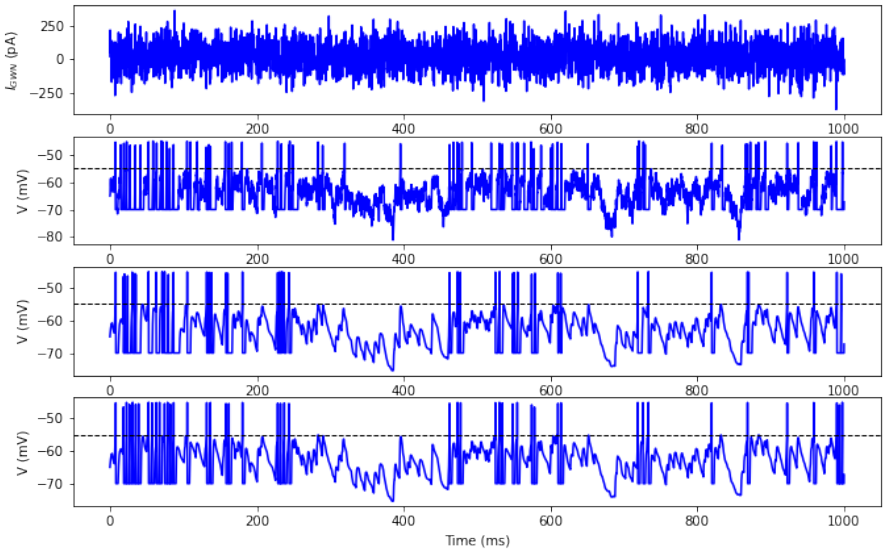

Figure 6. First row: Gaussian white noise current profile. Second row: Time evolution of membrane potential $V(t)$ with additive noise current $I_{\text{app}} = 23 + \eta(t)$ (pA) and random refractory period $t_{\text{ref}} = 3 + \tilde{\eta}(t)$ (ms). Third row: Time evolution of membrane potential $V(t)$ with direct input current $I_{\text{app}} = 23$ (pA) and with random refractory period $t_{\text{ref}} = 3 + \tilde{\eta}(t)$ (ms). Fourth row: Time evolution of membrane potential $V(t)$ with direct input current $I_{\text{app}} = 23$ (pA) and with direct refractory period $t_{\text{ref}} = 3$ (ms). Parameters: $\sigma_{\text{ref}} = 2$, $I_{\text{dbs}} = 0$ (pA).The dash line represents the spike threshold $V_{\text{th}} = -55$ (mV).

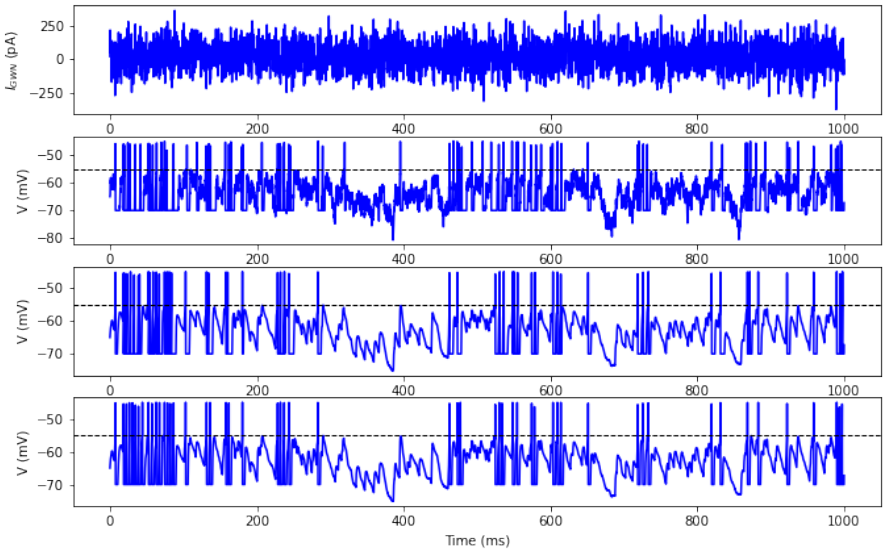

Figure 7. First row: Gaussian white noise current profile. Second row: Time evolution of membrane potential $V(t)$ with additive noise current $I_{\text{app}} = 23 + \eta(t)$ (pA) and random refractory period $t_{\text{ref}} = 3 + \tilde{\eta}(t)$ (ms). Third row: Time evolution of membrane potential $V(t)$ with direct input current $I_{\text{app}} = 23$ (pA) and with random refractory period $t_{\text{ref}} = 3 + \tilde{\eta}(t)$ (ms). Fourth row: Time evolution of membrane potential $V(t)$ with direct input current $I_{\text{app}} = 23$ (pA) and with direct refractory period $t_{\text{ref}} = 3$ (ms). Parameters: $\sigma_{\text{ref}} = 2$, $I_{\text{dbs}} = 2 + \sin(2\pi t)$ (pA). The dash line represents the spike threshold $V_{\text{th}} = -55$ (mV).

Since the plots of Figures 5–7 show high firing rates, we also provide the corresponding plots to zoom these figures in Figures 8–10 below. When we zoom Figures 5–7 in the time interval [50, 500] (ms), we observe that the random input current and random refractory period could cause not only silences but also bursts. This is visible in the first to rows of Figures 8–10.

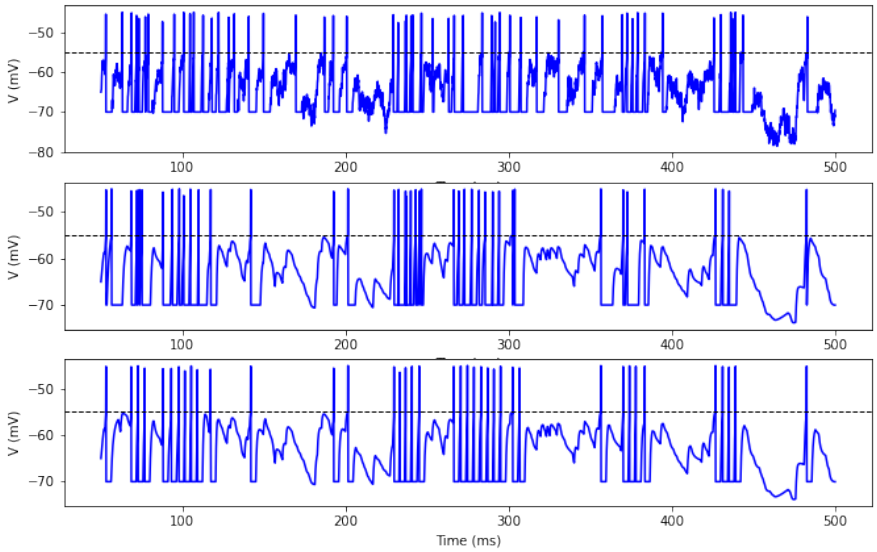

Figure 8. First row: Gaussian white noise current profile. Second row: Time evolution of membrane potential $V(t)$ with additive noise current $I_{\text{app}} = 23 + \eta(t)$ (pA) and random refractory period $t_{\text{ref}} = 3 + \tilde{\eta}(t)$ (ms). Third row: Time evolution of membrane potential $V(t)$ with direct input current $I_{\text{app}} = 23$ (pA) and with random refractory period $t_{\text{ref}} = 3 + \tilde{\eta}(t)$ (ms). Fourth row: Time evolution of membrane potential $V(t)$ with direct input current $I_{\text{app}} = 33$ (pA) and with direct refractory period $t_{\text{ref}} = 3$ (ms). Parameters: $\sigma_{\text{ref}} = 2$, $I_{\text{dbs}} = 0$ (pA). The dash line represents the spike threshold $V_{\text{th}} = -55$ (mV).

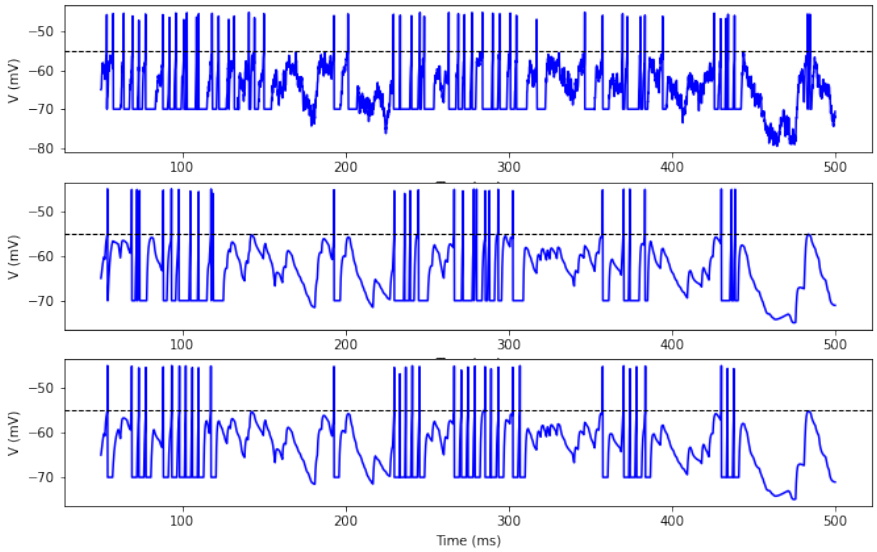

Figure 9. First row: Gaussian white noise current profile. Second row: Time evolution of membrane potential $V(t)$ with additive noise current $I_{\text{app}} = 23 + \eta(t)$ (pA) and random refractory period $t_{\text{ref}} = 3 + \tilde{\eta}(t)$ (ms). Third row: Time evolution of membrane potential $V(t)$ with direct input current $I_{\text{app}} = 23$ (pA) and with random refractory period $t_{\text{ref}} = 3 + \tilde{\eta}(t)$ (ms). Fourth row: Time evolution of membrane potential $V(t)$ with direct input current $I_{\text{app}} = 23$ (pA) and with direct refractory period $t_{\text{ref}} = 3$ (ms). Parameters: $\sigma_{\text{ref}} = 2$, $I_{\text{dbs}} = 0$ (pA). The dash line represents the spike threshold $V_{\text{th}} = -55$ (mV).

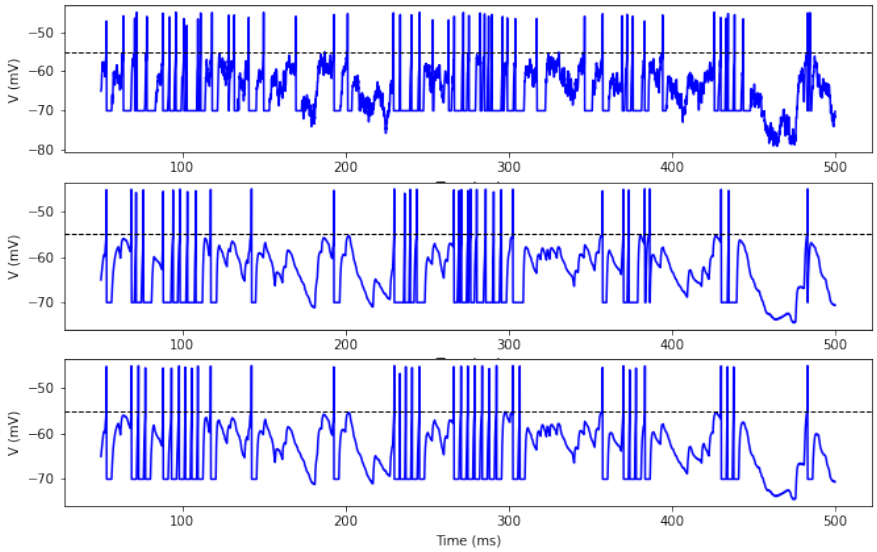

Figure 10. First row: Gaussian white noise current profile. Second row: Time evolution of membrane potential $V(t)$ with additive noise current $I_{\text{app}} = 23 + \eta(t)$ (pA) and random refractory period $t_{\text{ref}} = 3 + \tilde{\eta}(t)$ (ms). Third row: Time evolution of membrane potential $V(t)$ with direct input current $I_{\text{app}} = 23$ (pA) and with random refractory period $t_{\text{ref}} = 3 + \tilde{\eta}(t)$ (ms). Fourth row: Time evolution of membrane potential $V(t)$ with direct input current $I_{\text{app}} = 23$ (pA) and with direct refractory period $t_{\text{ref}} = 3$ (ms). Parameters: $\sigma_{\text{ref}} = 2$, $I_{\text{dbs}} = 2 + \sin(2\pi t)$ (pA). The dash line represents the spike threshold $V_{\text{th}} = -55$ (mV).

Further analysis for investigating the spiking activities is provided based on Figures 11–16, where we present the input-output transfer function and spike irregularity profiles of the neuron.

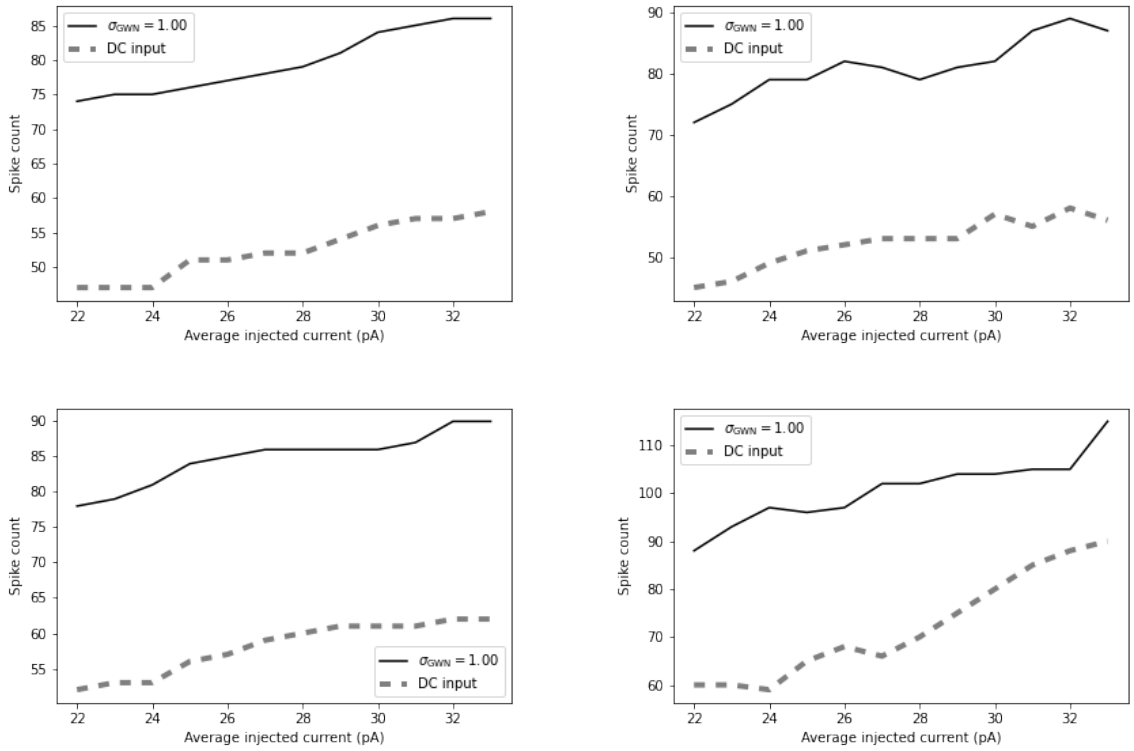

Figure 11. The input-output transfer function of the neuron with the output firing rate as a function of input mean for the case with additive noise input current ($\sigma_{\text{app}} = 1$). Top left panel: direct time refractory period $t_{\text{ref}} = 3$ (ms) with $I_{\text{dbs}} = 0$ (pA). Top right panel: random refractory period $t_{\text{ref}} = 3 + 2\tilde{\eta}(t)$ (ms) with $I_{\text{dbs}} = 0$. Bottom left panel: direct time refractory period $t_{\text{ref}} = 3$ (ms) with $I_{\text{dbs}} = 2 + \sin(2\pi t)$ (pA). Bottom right panel: random refractory period $t_{\text{ref}} = 3 + 2\tilde{\eta}(t)$ (ms) with $I_{\text{dbs}} = 5 + 5\sin(2\pi t)$ (pA).

The phenomena observed in Figures 5–7 are visible also in Figure 11. We have plotted the input-output transfer function of the neuron with the output firing as a function of average injected current in cases presented in Figures 5–7. We consider the values of average injected current belonging to the interval $I_{\text{average}} = [22, 34]$ (pA). This I_{average} quantity includes the values of healthy STN and PD-affected STN cells. We aim at revealing the dynamic behavior of the input-output transfer function of the neuron changing over a short interval including values switched from healthy to PD conditions. However, we look mainly at the values at $I_{\text{app}} = 23$ (pA) and $I_{\text{app}} = 33$ (pA). In our consideration, we first determine a set of current injection values to use as $I_{\text{average}} = [22, 34]$ (pA). Then, for each injection level, we count the number of spikes in milliseconds to determine the firing rate. Specifically, in the top left panel of Figure 11, by considering the direct refractory period we see that the presence of additive noise input current in the system increases the spiking activity of the STN neuron more than in the case of direct input current. Looking at the top right panel of Figure 11, it is clear that the presence of a random refractory period strongly affects the spiking activity in our system. There

are fluctuations in both cases of direct input current and additive noise input current. Moreover, in the presence of the random refractory period together with the random input current, the spiking activity of the neuron increases dramatically compared with the case presented in the top left panel of Figure 11. In the bottom left panel of Figure 11, we investigate also the case of injecting I_{dbs} current into the system. There is a significant increase in the spiking activity of the STN neuron. Furthermore, the spike count profiles in the case of direct input current look quite similar to those in both the top left and right panels of Figure 11. In the bottom right panel of Figure 11, at $I_{\text{app}} = 23$ (pA) and $I_{\text{app}} = 33$ (pA) with a DBS frequency input current, the firing activity is more efficient compared to the case presented in the bottom right panel of the same figure. In the presence of DBS frequency input current, we also observe that the contribution of the random refractory period makes the spiking activity of the STN neuron more efficient compared to the case with a direct refractory period.

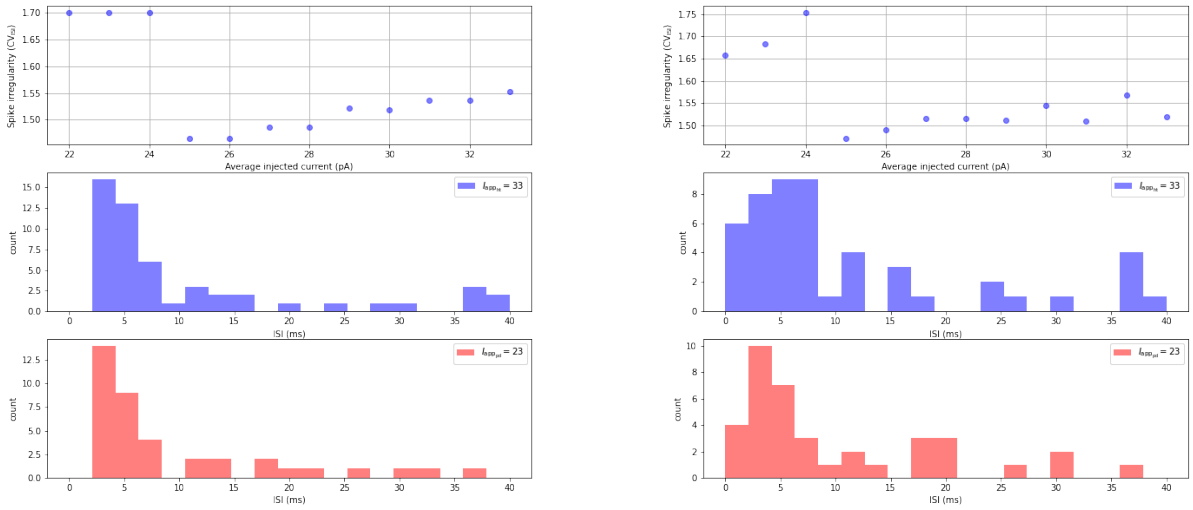

Figure 12. Spike irregularity profiles in the case with the direct input current and the ISI distribution. First column: direct time refractory period $t_{\text{ref}} = 3$ (ms). Second column: random refractory period $t_{\text{ref}} = 3 + \tilde{\eta}(t)$ (ms). Middle row: ISI distribution of a healthy cell. Last row: ISI distribution of a PD-affected cell.

In Figures 12–16, we look at the corresponding spike irregularity profile of the spike count in Figures 5–7. In general, the variability of the ISI is measured by its coefficient of variation CV_{ISI}. Our representative examples focus on the values at $I_{\text{app}} = 23$ (pA) and $I_{\text{app}} = 33$ (pA). We first determine a set of current injection values to use as $I_{\text{average}} = [22, 34]$ (pA). Next, the ISI is calculated by the following steps: calculate the spike times, and take the differences between spike times. Then, the CV_{ISI} is defined as in (2.22). In particular, in the top left panel of Figure 12, with direct input current and direct refractory period, we have high irregularity values of $CV_{\text{ISI}} = 1.7$ at the injected current values $I_{\text{app}} = 23$ (pA) and $CV_{\text{ISI}} = 1.5$ at the injected current values $I_{\text{app}} = 33$ (pA). In the top right panel of Figure 12, using direct input current with a random refractory period, we have values of CV_{ISI} similar to the case presented in the top left panel of the same figure. However now, there is a slight fluctuation due to the presence of the random refractory period. We look also at the ISI distribution

profiles of the two cases of healthy STN and PD-affected STN cells in the last two rows of Figure 12. We produce histograms of the ISI data, binned into 20 bins running from 0 to 40. The shapes of the histograms in Figure 12 approximate the exponential probability density function which is the probability density function for Poisson processes. Moreover, the spiking activity in both healthy and PD-affected STN cells in the case of a direct refractory period is more stable than in the case of a random refractory period.

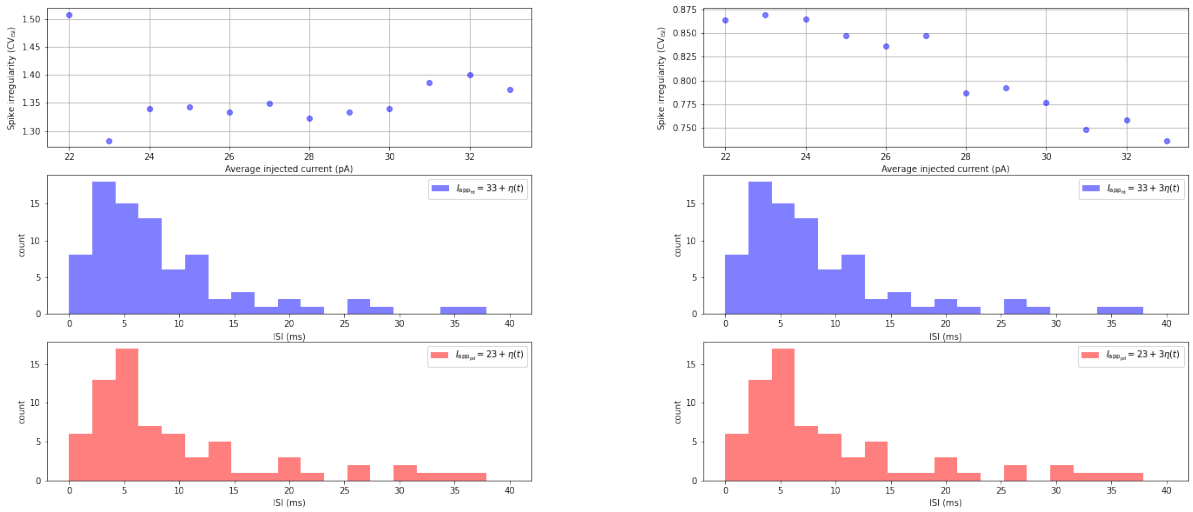

Figure 13. Spike irregularity profiles in the case with the additive noise input current and the ISI distribution. First column: random refractory period $t_{\text{ref}} = 3 + 2\tilde{\eta}(t)$ (ms) with $I_{\text{app}} = I_{\text{average}} + \eta(t)$. Second column: random refractory period $t_{\text{ref}} = 3 + 2\tilde{\eta}(t)$ (ms) with $I_{\text{app}} = I_{\text{average}} + 3\eta(t)$. Middle row: ISI distribution of a healthy cell in presence of Gaussian white noise $I_{\text{app}} = 33 + \eta(t)$ (pA). Last row: ISI distribution of a PD-affected cell in presence of Gaussian white noise $I_{\text{app}} = 23 + \eta(t)$ (pA).

In Figure 13, we consider the cases of random input current with different values of standard deviations and in the presence of random refractory period. In particular, in the top left panel of Figure 13, we see that there exist high irregularity values of the variability of the ISI with $CV_{\text{ISI}} = 1.3$ at the injected current values $I_{\text{app}} = 23$ (pA) and $CV_{\text{ISI}} = 1.37$ at the injected current values $I_{\text{app}} = 33$ (pA). However, when we increase the value of standard deviation σ_{app} from 1 to 3, the spike trains is more regular with $CV_{\text{ISI}} = 0.87 < 1$ (the Poisson train has $CV_{\text{ISI}} = 1$) at the injected current values $I_{\text{app}} = 23$ (pA) and $CV_{\text{ISI}} = 0.725$ at the injected current values $I_{\text{app}} = 33$ (pA). The shapes of histograms still approximate the exponential probability density function. There is a decrease of the spike irregularity coefficient CV_{ISI} from 1.3 to 0.87 ($I_{\text{app}} = 23$ (pA)) and from 1.37 to 0.725 ($I_{\text{app}} = 33$ (pA)) when we increase the values of σ_{app}. This is due to the fact that when we increase the standard deviation of the Gaussian white noise, at some point, the fluctuations of the random input current also increase. Hence, as the input is highly oscillating, the neuron is charged up to the spike threshold and then it is reset. This essentially gives an almost regular spiking.

In Figure 14, we examine the same quantities as in the cases presented in Figure 12. The only

difference is that we add a DBS frequency input current $I_{\text{dbs}} = 5 + 5\sin(2\pi t)$ (pA) into the system. The spike irregularity is slightly reduced in both cases: direct and random refractory periods compared with the cases presented in Figure. The shapes of the histograms in Figure 14 also approximate the exponential probability density function. We have an increase in the spiking activity of the neuron in the cases presented in Figure 14 compared with the cases presented in Figure 12.

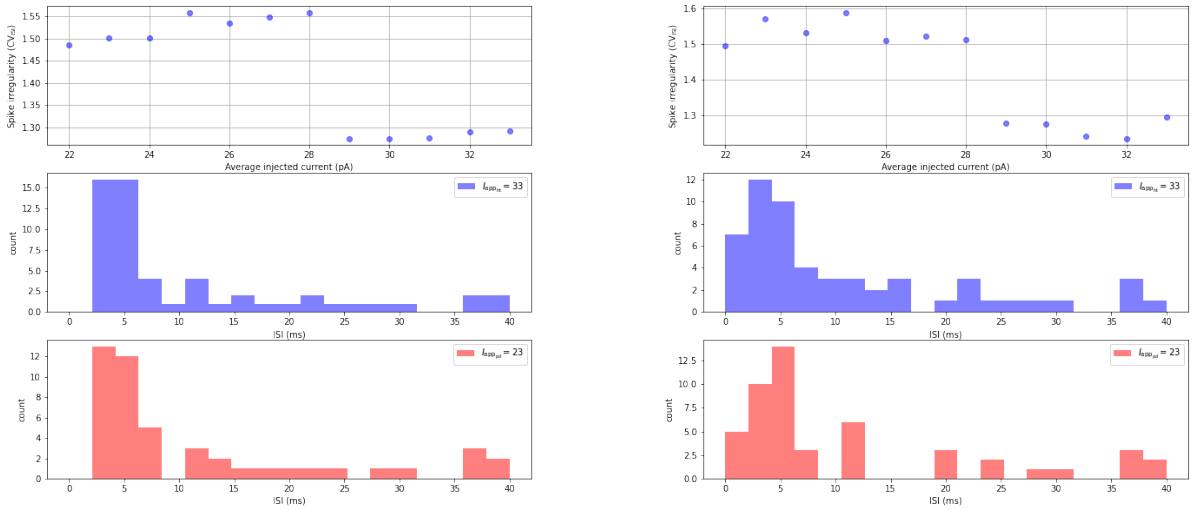

Figure 14. Spike irregularity profiles in the case with the additive noise input current and the ISI distribution. First column: direct time refractory period $t_{\text{ref}} = 3$ (ms) with $I_{\text{dbs}} = 5 + 5\sin(2\pi t)$ (pA). Second column: random refractory period $t_{\text{ref}} = 3 + \tilde{\eta}(t)$ (ms) with $I_{\text{dbs}} = 5 + 5\sin(2\pi t)$ (pA). Middle row: ISI distribution of a healthy cell. Last row: ISI distribution of a PD-affected cell.

In Figure 15, we consider the cases of direct refractory period in the presence of DBS frequency input current $I_{\text{dbs}} = 5 + 5\sin(2\pi t)$ (pA) together with random input current. In the first row of Figure 15, when we add random input currents into the system, the spike irregularity values are strongly reduced compared with the cases presented in Figure 12–14. In particular, in the top left panel of Figure 15, we have $CV_{\text{ISI}} = 0.625$ at the injected current value $I_{\text{app}} = 23$ (pA) and $CV_{\text{ISI}} = 0.51$ at the injected current value $I_{\text{app}} = 33$ (pA). This is caused by the presence of the DBS frequency input current which makes the spiking activity of the neuron increased. However, when we increase the value of σ_{app} from 1 to 3, the spike trains are more regular with $CV_{\text{ISI}} = 0.48 < 0.5$ at the injected current value $I_{\text{app}} = 23$ (pA) and $CV_{\text{ISI}} = 0.40 < 0.5$ at the injected current value $I_{\text{app}} = 33$ (pA). Note that increased ISI regularity could result in bursting [29]. The spike trains are substantially more regular with a range $CV_{\text{ISI}} \in (0; 0.5)$, and more irregular when $CV_{\text{ISI}} > 0.5$ [30]. Therefore, the presence of random input current with high oscilations could lead to the burst discharge.

In Figure 16, we analyze at the case of random refractory period in the presence of DBS frequency input current $I_{\text{dbs}} = 5 + 5\sin(2\pi t)$ (pA) together with random input current. In the top left panel of Figure 16, we see that the spike irregularity looks similar to the top left panel of Figure 15. However, when we increase the value of σ_{app} from 1 to 3, the spike irregularity increases compared with the

case presented in the top right panel of Figure 15. This phenomenon is quite interesting since the presence of random refractory periods could reduce the effects of random input currents on the system in the presence of DBS frequency input current. From the histograms in Figure 12–16 we see that their shapes approximate the exponential probability density function except the case presented in the right panel of the second row in Figure 16 for the healthy STN cell with a different shape. This is due to the effects of high fluctuations arising from random factors. However, the DBS treatment is commonly used in the case of Parkinsonian cells. Hence, in our consideration of DBS frequency input current, we have concentrated on the results of Parkinsonian conditions.

Additionally, we remark that the presence of the random refractory period and random input current affects the spiking activity of the STN neuron even in the presence of the DBS frequency input current. When we increase values of the standard deviation in random input currents and random refractory periods, the irregularity of spike trains decreases. This effect may lead to an improvement in the carrying out the information about stimulating activities in the neuron (see also, e.g., [31]). Furthermore, the presence of random refractory periods could reduce the effects of random input currents on the system in presence of DBS frequency input current. The interplay between random refractory period and random input current in the STN cell membrane potential would contribute to further progress and model developments for the DBS therapy.

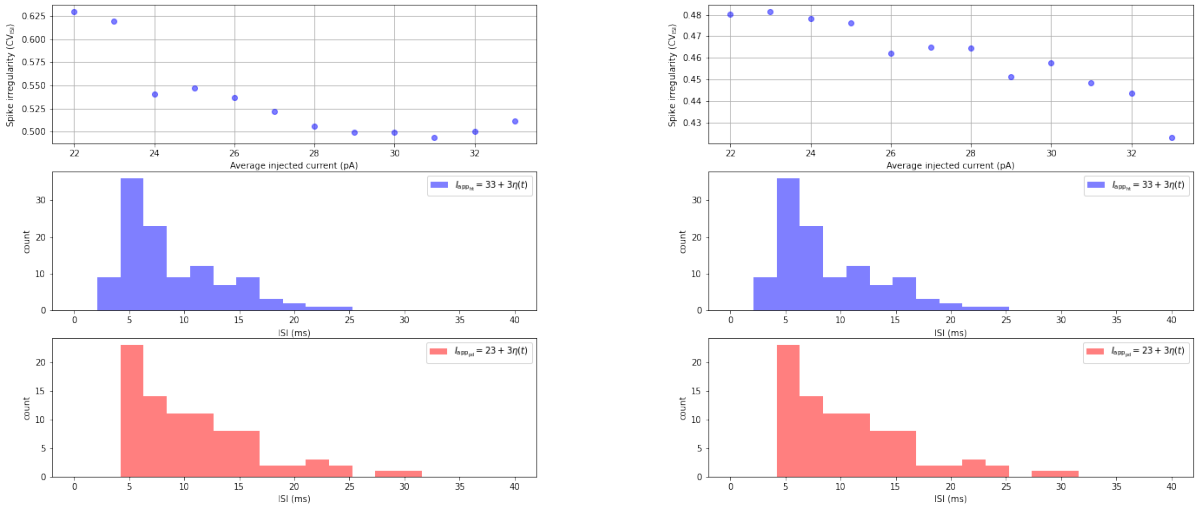

Figure 15. Spike irregularity profiles in the case with the additive noise input current and the ISI distribution. First column: direct time refractory period $t_{\text{ref}} = 3$ (ms) with $I_{\text{dbs}} = 5 + 5\sin(2\pi t)$ (pA). Second column: direct time refractory period $t_{\text{ref}} = 3$ (ms) with $I_{\text{dbs}} = 5 + 5\sin(2\pi t)$ (pA). Middle row: ISI distribution of a healthy cell in presence of Gaussian white noise $I_{\text{app}} = 33 + \eta(t)$ (pA) (left) and $I_{\text{app}} = 33 + 3\eta(t)$ (pA) (right). Last row: ISI distribution of a PD-affected cell in presence of Gaussian white noise $I_{\text{app}} = 23 + \eta(t)$ (pA) (left) and $I_{\text{app}} = 23 + 3\eta(t)$ (pA) (right).

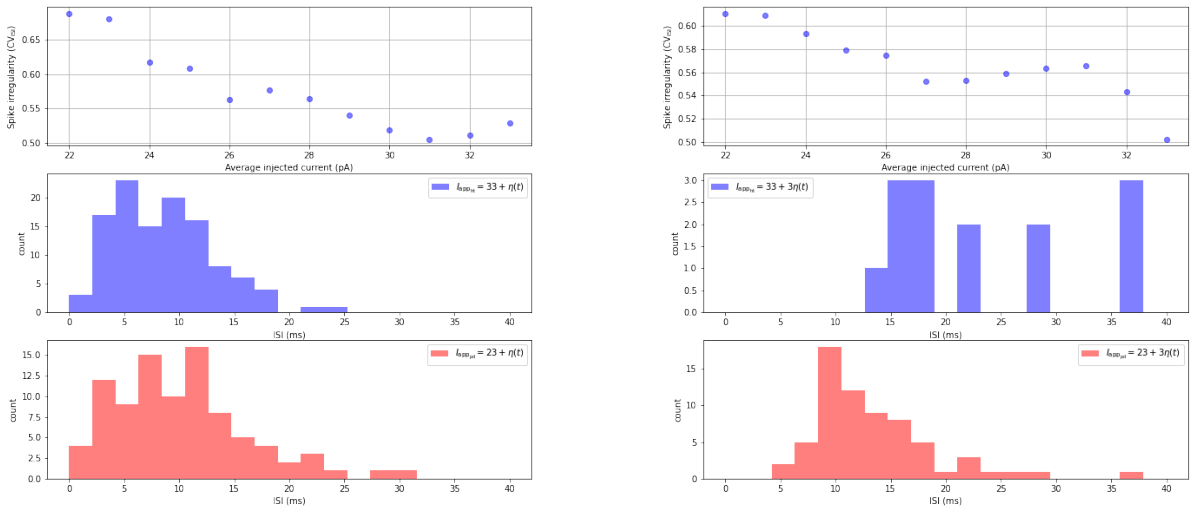

Figure 16. Spike irregularity profiles in the case with the additive noise input current and the ISI distribution. First column: random refractory period $t_{\text{ref}} = 3 + 2\tilde{\eta}(t)$ (ms) with $I_{\text{dbs}} = 2 + \sin(2\pi t)$ (pA). Second column: random refractory period $t_{\text{ref}} = 3 + 2\tilde{\eta}(t)$ (ms) with $I_{\text{dbs}} = 2 + \sin(2\pi t)$ (pA). Middle row: ISI distribution of a healthy cell in presence of Gaussian white noise $I_{\text{app}} = 33 + \eta(t)$ (pA) (left) and $I_{\text{app}} = 33 + 3\eta(t)$ (pA) (right). Last row: ISI distribution of a PD-affected cell in presence of Gaussian white noise $I_{\text{app}} = 23 + \eta(t)$ (pA) (left) and $I_{\text{app}} = 23 + 3\eta(t)$ (pA) (right).

4. Conclusions

We have proposed a new modified HH model and described the process of synaptic conductance with random inputs. Using the description based on Langevin stochastic dynamics in a numerical setting, we analyzed the effects of random inputs in an STN cell membrane potential. Specifically, we provided details of the corresponding models along with representative numerical examples and discussed the effects of random inputs on the time evolution of the cell membrane potentials, the associated spiking activities of neurons and the spike time irregularity profiles. Our numerical results have shown that the random inputs strongly affect the spiking activities of neurons in the STN even in the presence of DBS in the system. Furthermore, we have shown that an increase in the standard deviations in the random input current can lead to a decreased irregularity of spike trains of the output neuron. However, the presence of a random refractory period together with the random input current can increase the irregularity of spike trains of the output neuron. More efficient managing of random factors in STN cell membrane potential models would allow for further improvements of smart treatments and bioengineering technique modalities for PD. A better understanding of cell membrane potential models developed for the targeted area of the brain that is responsible for the movement symptoms caused by PD would allow for supporting and improving the DBS therapy and other applications in the fields of biomedicine.

Acknowledgment

Authors are grateful to the NSERC and the CRC Program for their support. RM is also acknowledging support of the BERC 2022-2025 program and Spanish Ministry of Science, Innovation and Universities through the Agencia Estatal de Investigacion (AEI) BCAM Severo Ochoa excellence accreditation SEV-2017-0718 and the Basque Government fund AI in BCAM EXP. 2019/00432.

Conflict of interest

The Authors declare that there is no conflict of interest.

References

1. Yang YC, Tai CH, Pan MK, et al. (2014) The T-type calcium channel as a new therapeutic target for Parkinson's disease. *Pflugers Arch - Eur J Physiol* 446: 747–755. https://doi.org/10.1007/s00424-014-1466-6
2. Shaheen H and Melnik R (2022) Deep brain stimulation with a computational model for the cortex-thalamus-basal-ganglia system and network dynamics of neurological disorders. *Compu Math Method* 2022: 8998150. https://doi.org/10.1155/2022/8998150
3. Sjöström PJ (2021) Grand challenge at the frontiers of synaptic neuroscience. *Front Synaptic Neurosci* 13: 748937. https://doi.org/10.3389/fnsyn.2021.748937
4. Shaheen H, Singh S, Melnik R (2021) A neuron-glial model of exosomal release in the onset and progression of Alzheimer's disease. *Front Comput Neurosci* 15: 653097. https://doi.org/10.3389/fncom.2021.653097
5. Huang CS, Wang GH, Chuang HH, et al. (2021) Conveyance of cortical pacing for parkinsonian tremor-like hyperkinetic behavior by subthalamic dysrhythmia. *Cell Rep* 35: 109007. https://doi.org/10.1016/j.celrep.2021.109007
6. Boag MK, Ma L, Mellick GD, et al. (2021) Calcium channels and iron metabolism: A redox catastrophe in Parkinson's disease and an innovative path to novel therapies?. *Redox Biol* 47: 102136. https://doi.org/10.1016/j.redox.2021.102136
7. Ortner NJ (2021) Voltage-gated Ca2+ channels in dopaminergic substantia Nigra neurons: Therapeutic targets for neuroprotection in Parkinson's disease?. *Front Synaptic Neurosci* 13: 636103. https://doi.org/10.3389/fnsyn.2021.636103
8. Puckerin AA, Chang DD, Shuja Z, et al. (2018) Engineering selectivity into RGK GTPase inhibition of voltage-dependent calcium channels. *PNAS* 115: 12051–12056. https://doi.org/10.3389/fnsyn.2021.636103
9. Chen X, Xue B, Wang J, et al. (2018) Potassium channels: A potential therapeutic target for Parkinson's disease. *Neurosci Bull* 34: 341–348. https://doi.org/10.1007/s12264-017-0177-3
10. Zhang L, Zheng Y, Xie J, et al. (2020) Potassium channels and their emerging role in parkinson's disease. *Brain Res Bull* 160: 1–7. https://doi.org/10.1016/j.brainresbull.2020.04.004

11. Powanwe AS and Longtin A (2021) Brain rhythm bursts are enhanced by multiplicative noise. *Chaos* 31: 013117. https://doi.org/10.1063/5.0022350

12. Zheng T, Kotani K, Jimbo Y (2021) Distinct effects of heterogeneity and noise on gamma oscillation in a model of neuronal network with different reversal potential. *Sci Rep* 11: 12960. https://doi.org/10.1038/s41598-021-91389-8

13. Faisal AA, Selen LPJ, Wolpert DM (2008) Noise in the nervous system. *Nat Rev Neurosci* 9: 292–303. https://doi.org/10.1038/nrn2258

14. Thieu TKT and Melnik R (2022) Effects of random inputs and short-term synaptic plasticity in a LIF conductance model for working memory applications. In: Rojas I, Valenzuela O, Rojas F, et al., *Bioinformatics and Biomedical Engineering,* Cham: Springer, 59–72. https://doi.org/10.48550/arXiv.2205.04655

15. van der Groen O, Mattingley JB, Wenderoth N (2019) Altering brain dynamics with transcranial random noise stimulation. *Sci Rep* 9: 4029. https://doi.org/10.1038/s41598-019-40335-w

16. Lautenschläger J, Stephens AD, Fusco G, et al. (2018) C-terminal calcium binding of α-synuclein modulates synaptic vesicle interaction. *Nat Commun* 9: 712. https://doi.org/10.1038/s41467-018-03111-4

17. So RQ, Kent AR, Grill WM (2012) Relative contributions of local cell and passing fiberactivation and silencing to changes in thalamic fidelity during deep brain stimulation and lesioning: a computational modeling study. *J Comput Neurosci* 32: 499–519. https://doi.org/10.1007/s10827-011-0366-4

18. Gerstner W, Kistler WM, Naud R, et al. (2014) Neuronal dynamics: from single neurons to networks and models of cognition. New York: Cambridge University Press. https://doi.org/10.1017/CBO9781107447615

19. Dayan P and Abbott LF (2005) Theoretical Neuroscience. The MIT Press Cambridge, Massachusetts London, England. https://doi.org/10.1017/CBO9781107447615

20. Li S, Liu N, Yao L, et al. (2019) Determination of effective synaptic conductances using somatic voltage clamp. *PLoS Comput Biol* 15: e1006871. https://doi.org/10.1371/journal.pcbi.1006871

21. Chiken S and Nambu A (2016) Mechanism of deep brain stimulation: inhibition, excitation, or disruption?. *The Neuroscientist* 22: 313–322. https://doi.org/10.1177/1073858415581986

22. Cornelisse LN, Scheenen WJJM, Koopman WJH, et al. (2001) Minimal model for intracellular calcium oscillations and electrical bursting in melanotrope cells of Xenopus Laevis. *Neural Comput* 13: 113–137. https://doi.org/10.1162/089976601300014655

23. Traub RD, Wong RK, Miles R, et al. (1999) A model of CA3 hippocampal pyramidal neuron incorporating voltage-clamp data on intrinsic conductances. *J Neurophysiol* 66: 635–650. https://doi.org/10.1152/jn.1991.66.2.635

24. Roberts JA, Friston KJ, Breakspear M (2017) Clinical applications of stochastic dynamic models of the brain, Part I: a primer. *Biol Psychiatry-Cogn N* 2: 216–224. https://doi.org/10.1016/j.bpsc.2017.01.010

25. Teka W, Marinov TM, Santamaria F (2004) Neuronal integration of synaptic input in the fluctuation-driven regime. *J Neurosci* 24: 2345–2356. https://doi.org/10.1523/JNEUROSCI.3349-03.2004

26. Gallinaro JV and Clopath C (2021) Memories in a network with excitatory and inhibitory plasticity are encoded in the spiking irregularity. *PLoS Comput Biol* 17: e1009593. https://doi.org/10.1371/journal.pcbi.1009593

27. Christodoulou C and Bugmann G (2001) Coefficient of variation vs. mean interspike interval curves: What do they tell us about the brain?. *Neurocomputing* 38-40: 1141–1149. https://doi.org/10.1016/S0925-2312(01)00480-5

28. Breakspear M (2017) Dynamic models of large-scale brain activity. *Nat Neurosci* 20: 340–352. https://doi.org/10.1038/nn.4497

29. Maimon G and Assad JA (2009) Beyond poisson: increased spike-time regularity across primate parietal cortex. *Neuron* 62: 426–440. https://doi.org/10.1016/j.neuron.2009.03.021

30. Stiefel KM, Englitz B, Sejnowski TJ (2013) Origin of intrinsic irregular firing in cortical interneurons. *PNAS* 110: 7886–7891. https://doi.org/10.1073/pnas.1305219110

31. Bauermann J and Lindner B (2019) Multiplicative noise is beneficial for the transmission of sensory signals in simple neuron models. *BioSystems* 178: 25–31. https://doi.org/10.1016/j.biosystems.2019.02.002

AIMS Press